JOURNAL OF PROPULSION AND POWER
Vol. 9, No. 5, Sept.–Oct. 1993

Analysis and Design of an Ultrahigh Temperature Hydrogen-Fueled MHD Generator

Jeffrey P. Moder,* Leik N. Myrabo,† and Deborah A. Kaminski‡
Rensselaer Polytechnic Institute, Troy, New York 12180

A coupled gas dynamics/radiative heat transfer analysis of partially ionized hydrogen, in local thermodynamic equilibrium, flowing through an ultrahigh temperature (10,000–20,000 K) magnetohydrodynamic (MHD) generator is performed. Gas dynamics are modeled by a set of quasi-one-dimensional, nonlinear differential equations which account for friction, convective and radiative heat transfer, and the interaction between the ionized gas and applied magnetic field. Radiative heat transfer is modeled using nongray, absorbing-emitting, two- and three-dimensional P-1 approximations which permit an arbitrary variation of the spectral absorption coefficient with frequency. Gas dynamics and radiative heat transfer are coupled through the energy equation and through the temperature- and density-dependent absorption coefficient. The resulting nonlinear elliptic problem is solved by iterative methods. Design of such MHD generators as onboard, open-cycle, electric power supplies for a particular advanced airbreathing propulsion concept produced an efficient and compact 128-MW_e generator characterized by an extraction ratio (electric power extracted from the gas flow to total power into the gas) of 35.5%, a power density of 10,500 MW_e/m^3 and a specific (extracted) energy of 324 MJ_e/kg of hydrogen. The maximum wall heat flux and total wall heat load were 453 MW/m^2 and 62 MW, respectively.

Nomenclature

A = cross-sectional area, D_zD_y
a_ω = spectral absorption coefficient
$\boldsymbol{B}$ = magnetic induction vector, $\|\boldsymbol{B}\|$
C_P = $(\partial h/\partial T)_P$
C_T = $(\partial h/\partial P)_T$
c_s = sound speed
D_e = exit height of generator duct
D_i = entrance height of generator duct
D_P = $(\partial \rho/\partial T)_P$
D_T = $(\partial \rho/\partial P)_T$
D_y = constant width of generator duct
D_z = local height of generator duct
dB/B = $(\mu_0 \bar{J}_y D_z)/(2B)$
$\boldsymbol{E}$ = electric field vector
E_y = electric field due to external load
e_b = blackbody emissive power
$\bar{f}$ = value of function $f(x, y, z)$ averaged over $A(x)$, $\bar{f} = 1/A \iint f\, dA$
G = nonuniformity factor
g_α = partial molal Gibbs function of species α
H_R = extraction ratio, w_{tot}/Q_N
H_0 = stagnation enthalpy/mass
h = enthalpy/mass
I_0 = solid angle-integrated radiative intensity
$\boldsymbol{J}$ = conduction current density vector
J_y = Faraday current density
K = loading parameter, $\bar{E}_y/\bar{u}B$
k = Boltzmann constant
L = axial length of generator duct
L_c = axial length of conical duct
L_{ent} = entrance length required for fully developed flow at generator entrance
l_{mb} = mean beam length, $4V_{gen}/S_{gen}$
M = Mach number
m = number of axial nodes
$\dot{m}$ = mass flow rate of hydrogen through generator
max( ) = maximum value within generator
min( ) = minimum value within generator
$\hat{\boldsymbol{n}}_s$ = unit vector outward normal to surface s
$\mathcal{O}$ = optical thickness based on l_{mb}
P = static pressure
p = perimeter of generator duct, $2(D_y + D_z)$
Q_N = energy required to heat hydrogen to $\bar{T}_i$
Q_{rad} = radiative volume heat loss/mass from generator entrance to current x location
Q_{tot} = total volume heat loss/mass from generator
Q_w = heat/mass absorbed by generator walls from entrance to current x location
$Q_{w,tot}$ = total heat loss/mass to generator walls
$\boldsymbol{q}$ = heat flux vector
q_w = perimeter-averaged heat flux into walls
R = under-relaxation factor for iterative method
Re_{avg} = $1/L \int_0^L \rho_e(x)u_e(x)(x + L_{ent})/\mu_e(x)\, dx$
r_w = local radius of conical duct
S_E = energy sink term, Eq. (9)
S_{gen} = surface area of gas in generator duct
S_M = momentum sink term, Eq. (8)
s_{rad} = radiative sink term, $\nabla \cdot \boldsymbol{q}_{rad}$
T = static temperature
T_s = temperature of surface s
T_w = temperature of generator walls
u = velocity component in the x direction
$\boldsymbol{V}_f$ = fluid velocity
V_{gen} = volume of generator interior
$V(\Delta x)$ = volume of gas over length Δx
$\dot{W}_{gen}$ = electric power produced, $\dot{m}w_{tot}$
w = electric work/mass produced by generator from entrance to current x location
w_{tot} = total electric work/mass produced
x, r = cylindrical coordinates

Received Nov. 27, 1990; revision received Sept. 9, 1992; accepted for publication Dec. 1, 1992.

*Graduate Student; currently at NASA Lewis Research Center, M/S 5-11, 21000 Brookpark Rd., Cleveland, OH 44135. Member AIAA.

†Associate Professor, Department of Mechanical Engineering, Aeronautical Engineering and Mechanics. Member AIAA.

‡Associate Professor, Department of Mechanical Engineering, Aeronautical Engineering and Mechanics.

x, y, z = rectangular coordinates
β_e = Hall parameter for electrons
ΔQ_{rad} = radiative volume heat loss/mass over axial length Δx, $1/\dot{m} \iiint_{V(\Delta x)} s_{\text{rad}}\, dV$
ΔQ_w = heat/mass absorbed by generator walls over axial length Δx, $1/\dot{m} \int_{\Delta x} q_w p(x)\, dx$
ε_s = emissivity of surface s
ε_w = emissivity of gray-diffuse generator walls
θ = divergence half-angle, $2 \tan \theta(x) = dD_z/dx$
λ = thermal conductivity
μ = viscosity
μ_0 = permeability of free space
ρ = mass density
σ = electrical conductivity
τ_w = shear stress in gas at generator walls
ω = photon energy

Subscripts

c = property along duct centerline
ch = value at plasma generation chamber inlet
cond = conduction quantity
conv = convective heat transfer quantity
e = value at generator exit, property of electrons
h = property of heavy-particle species as a whole
i = value at generator inlet
j = quantity integrated over ω-band j
k = axial node
rad = radiative heat transfer quantity
s = property of surface s
w = property of generator wall
ω = photon energy dependent quantity

Introduction

THEORETICAL analysis and optimal design are performed for a particular class of magnetohydrodynamic (MHD) generators evisioned as lightweight, compact and efficient, open-cycle electric power supplies for several beamed-energy airbreathing-propulsion concepts. Hydrogen is chosen as the working fluid in order to maximize the specific impulse of the vehicle carrying the MHD generator(s) and enters the generator(s) in local thermodynamic equilibrium (LTE) at degrees of ionization exceeding 20% and temperatures near 20,000 K. For such conditions, high electric power levels may be achieved without seeding (adding small amounts of an easily ionized substance such as cesium or potassium into the working fluid) and, theoretically, such generators have the potential for power densities of 10,000+ MW_e/m^3 and specific energy levels of 300+ MJ_e/kg.

The complete power supply system consists of an energy source, plasma generation system, storage tank and pumping system for the working fluid, system for producing the applied magnetic field, and MHD generator. Hydrogen fuel is stored as liquid parahydrogen and used to regeneratively cool MHD generator walls and possibly other hot surfaces in the power supply. Before entering the MHD generator, the hydrogen is further heated to plasma, an ultrahigh equilibrium temperature which typically remains completely dissociated throughout the generator duct, except near the cool generator walls. Absorption of beamed-energy from a remote source into the hydrogen gas by a standing laser-supported plasma wave,[1,2] or a linear array of such waves, is considered the optimum energy source/plasma generation system for propulsive applications. The applied magnetic field (1–10 T) is produced by superconducting coils wound around the outside of the generator duct.

The MHD generator analyzed, shown in Fig. 1, is a Faraday generator with segmented electrode walls and separate electrical loads connected across each anode-cathode pair, the nature of which depend on the application. The cross section of the generator duct is rectangular, with D_y and D_z. The primary gas flow u is in the x direction, the applied magnetic field B is in the z direction, and the induced J_y, resulting from the flow of the partially ionized gas perpendicular to the applied field B, is in the negative y direction. In general, an axial or Hall current density J_x will also be present, causing a smaller current density J_y, and therefore, a loss in generator performance.

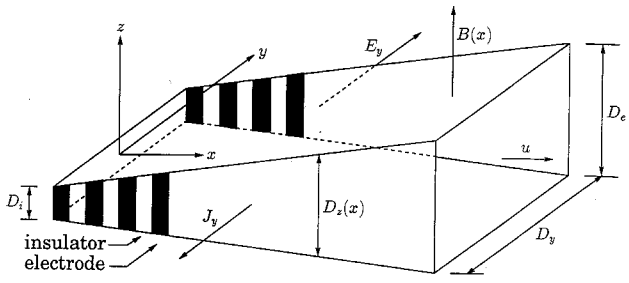

Fig. 1 MHD generator geometry.

A good measure of efficiency for high-temperature, open-cycle MHD generators is the extraction ratio, $H_R = w_{\text{tot}}/Q_N$. The maximum possible temperature of the hydrogen entering the plasma generation chamber is T_w. Ignoring any irreversibilities or heat loss in heating the hydrogen from T_w to T_i, the minimum value for Q_N is given by

$$Q_N = H_{0,i} - H_{0,\text{ch}} \tag{1}$$

The initial idea for ultrahigh temperature, hydrogen-fueled MHD generators as power supplies for beamed-energy propulsive engines was conceived by Myrabo.[3] No detailed analysis of such generators was undertaken and the emphasis was on repetitively pulsed, explosively driven, nonequilibrium MHD generators heated by laser-supported detonation waves (a supersonic plasma zone propagating along a high intensity energy beam). Rosa and Myrabo[4] discussed the potential of high-temperature (3000–10,000 K), closed-cycle MHD generators designed as onboard electric power supplies for mission payload and/or propulsive engines.

This study performs a coupled gas dynamics/radiative heat transfer analysis of partially ionized hydrogen, in LTE, flowing through a particular class of Faraday MHD generators. Radiative transport in the nonisothermal, essentially nonscattering, hydrogen gas is described using two- and three-dimensional, nongray P-1 approximations in which the directional dependence of the radiative intensity is approximated by a truncated set of spherical harmonics. Gas dynamics are described by a set of quasi-one-dimensional differential equations, which account for friction, convective and radiative heat losses, and the interaction between the ionized gas and the applied magnetic field. Local gas properties, as well as convective and radiative wall heat fluxes, total heat loss from the gas, and total electric work extracted from the gas flow, are evaluated by the computational models describing the gas dynamics and radiative transport.

The design of efficient MHD generators is formulated as an optimization problem in which the extraction ratio is maximized subject to several constraints. A numerical optimization code is used to find local optima within the feasible design space, given some approximation of the actual radiative loss distribution within the generator. Coupled gas dynamics/radiative heat transfer solutions for some of these designs are found and results for a near-optimal design are presented.

Analysis of Gas Dynamics

Governing Equations

The high pressures which exist throughout most of the generator allow the partially ionized hydrogen gas to be considered in LTE. Also, for typical conditions, the gas as a whole may be treated as an electrically neutral continuum, except

for a small sheath layer near the walls. Thus, the flow is adequately modeled by a single set of global continuum equations consisting of the conservation of mass, linear momentum, and energy.

For gaseous media, the relative permeability and permittivity of the gas are approximately equal to their free space values, so the Maxwell equation for $\boldsymbol{B}$ in a moving gas is given by

$$\nabla \times \boldsymbol{B} = \mu_0 \boldsymbol{J} \tag{2}$$

where the vacuum displacement current is negligible compared to conduction currents for typical generator conditions. The nonzero contribution to $\nabla \times \boldsymbol{B}$ is due only to electric currents within the gas since the component of $\boldsymbol{B}$ due to the external field coils is irrotational within the generator. Dividing Eq. (2) by B and approximating $(\nabla \times \boldsymbol{B})_y$ by $-\mathrm{d}B/(\frac{1}{2}D_z)$ leads to the parameter $\mathrm{d}B/B$, which is a measure of the distortion of the magnetic field due to internal currents $\bar{J}_y$. In the analysis which follows, distortion of the applied magnetic field is neglected and Eq. (2) is not required if $\mathrm{d}B/B$ is less than 0.1.

Also, for typical MHD generator conditions, the ion diffusion velocity contribution to the current density and the electron pressure gradient contribution to the effective electric field acting on an electron are negligible.[5] Neglecting thermal diffusion effects as well, the conduction current density and conduction heat flux vectors are given by[6]

$$\boldsymbol{J} = \vec{\bar{\sigma}}_e \cdot (\boldsymbol{E} + \boldsymbol{V}_f \times \boldsymbol{B}) \tag{3}$$

$$\boldsymbol{q}_{\text{cond}} = -\frac{5}{2}\frac{kT}{e}\boldsymbol{J} - \vec{\bar{\lambda}} \cdot \nabla T \tag{4}$$

The electron gas contribution to the viscous stress tensor can be neglected since the momentum of heavy-particle species is not significantly altered by collisions with electrons; thus, the viscous stress tensor can be expressed in terms of a single scalar viscosity.

For a Cartesian coordinate system in which the z coordinate is aligned with $\boldsymbol{B}$, the electron electrical conductivity tensor appearing in Eq. (3) is given by

$$\vec{\bar{\sigma}}_e = \begin{bmatrix} \sigma_{e,\perp} & -\sigma_{e,H} & 0 \\ \sigma_{e,H} & \sigma_{e,\perp} & 0 \\ 0 & 0 & \sigma_e \end{bmatrix} \tag{5}$$

and the thermal conductivity tensor is given by

$$\vec{\bar{\lambda}} = \begin{bmatrix} \lambda_{e,\perp} & -\lambda_{e,H} & 0 \\ \lambda_{e,H} & \lambda_{e,\perp} & 0 \\ 0 & 0 & \lambda_e \end{bmatrix} + \begin{bmatrix} \lambda_n & 0 & 0 \\ 0 & \lambda_h & 0 \\ 0 & 0 & \lambda_h \end{bmatrix} \tag{6}$$

The tensor components $\sigma_{e,\perp}$, $\sigma_{e,H}$, $\lambda_{e,\perp}$, and $\lambda_{e,H}$ depend on the local magnetic field value, as well as the state of the gas. Lacking accurate data for these transport properties at various gas temperatures, pressures and magnetic field values, the following approximations are employed:

$$\lambda_{e,\perp} = \lambda_e \frac{1}{1+\beta_e^2} \quad \text{and} \quad \lambda_{e,H} = \lambda_e \frac{\beta_e}{1+\beta_e^2}$$

$$\sigma_{e,\perp} = \sigma_e \frac{1}{1+\beta_e^2} \quad \text{and} \quad \sigma_{e,H} = \sigma_e \frac{\beta_e}{1+\beta_e^2}$$

where σ_e and λ_e are the ordinary scalar electrical and thermal electron conductivities. Mitchner and Kruger[6] show that the above approximations for $\lambda_{e,\perp}$ and $\lambda_{e,H}$, and $\sigma_{e,\perp}$ and $\sigma_{e,H}$ may only be accurate within a factor of 2.

The entrance gas flow of the MHD generator is assumed to be a steady, fully developed turbulent flow. This is probably the most unfavorable entrance flow possible with respect to minimizing heat and friction losses. It is assumed that the flow remains turbulent throughout the generator and shear stress and conductive heat flux are calculated based on ordinary hydrodynamic turbulence models. No attempt is made here to include the effect of the applied magnetic field on gas flow turbulence.

To simplify the gas dynamics analysis, the governing equations are integrated over $A(x)$. The applied magnetic field B is only a function of the axial coordinate x and has only a z component. The viscous shear stress is assumed to be uniform along the generator perimeter at a given x location, and pressure is assumed to be a function of x only. The convective heat flux is assumed to be uniform along portions of the generator perimeter at a given x location; due to the anisotropy of the thermal conductivity, the uniform value of the heat flux along the walls $y = -D_y/2$ and $y = D_y/2$ differs from the uniform value along the walls $z = -D_z/2$ and $z = D_z/2$. The electrode walls are assumed to be infinitely segmented so that the cross-sectionally averaged Hall current $\bar{J}_x = 0$, although an average Hall electric field $\bar{E}_x$ is present. Finally, making some assumptions consistent with the velocity and temperature profile shapes in an ordinary hydrodynamic turbulent flow, integration of the governing equations over $A(x)$ yields the following set of quasi-one-dimensional MHD equations[7,8]:

$$\bar{\rho}\bar{u}A = \dot{m} \quad \text{or} \quad \frac{1}{\bar{\rho}}\frac{\mathrm{d}\bar{\rho}}{\mathrm{d}x} + \frac{1}{\bar{u}}\frac{\mathrm{d}\bar{u}}{\mathrm{d}x} + \frac{1}{A}\frac{\mathrm{d}A}{\mathrm{d}x} = 0 \tag{7}$$

$$\bar{\rho}\bar{u}\frac{\mathrm{d}\bar{u}}{\mathrm{d}x} + \frac{\mathrm{d}P}{\mathrm{d}x} = -\left[\tau_w \frac{p}{A} + \bar{J}_y B\right] = -S_M \tag{8}$$

$$\bar{\rho}\bar{u}\frac{\mathrm{d}}{\mathrm{d}x}\left(\bar{h} + \frac{1}{2}\bar{u}^2\right) = -\left[\bar{J}_y\bar{E}_y + q_{w,\text{conv}}\frac{p}{A} + \bar{s}_{\text{rad}}\right] = -S_E \tag{9}$$

$$\bar{J}_y = \frac{\bar{\sigma}_e}{G}\bar{u}B(1-K) \tag{10}$$

where the nonuniformity factor[7,8] $G \sim 1.2$ for typical generator conditions and the approximations $\bar{\rho} \approx \rho(\bar{T}, P)$, $\bar{h} \approx h(\bar{T}, P)$, and $\bar{\sigma}_e \approx \sigma_e(\bar{T}, P)$ are used.

In the above equations, all flow quantities represent Reynolds-averaged mean turbulent quantities, except B. K is determined by the external electrical load at a given axial location. For analysis, this parameter is treated as a constant since a large variation in K is not typical of well-designed MHD generators. All quantities in the above equations are positive, except the radiative volume loss term $\bar{s}_{\text{rad}}$ and the energy sink term S_E, which may be positive or negative.

Calculation of $\tau_w(x)$ and $q_{w,\text{conv}}(x)$ assumes a steady, compressible, turbulent, flat-plate boundary-layer flow exists locally over each generator wall. Values for viscosity, (scalar) thermal conductivity, and (scalar) electrical conductivity of hydrogen at temperatures of 1000–26,000 K, and pressures of 1–30 atm are approximated by curve fits of data produced by Yos.[9] Extrapolation of this data to pressures above 30 atm and below 1 atm is necessary for the analysis of several MHD generator designs. Details of the curve-fitting procedure employed and of the calculation of τ_w and $q_{w,\text{conv}}$ are presented in Ref. 7.

Calculation of the composition of hydrogen in LTE is accomplished by applying the equation of reaction equilibrium (i.e., $g_{H_2} = 2g_H$ and $g_H = g_{H^+} + g_e$) to the dissociation and ionization reactions $H_2 \rightleftharpoons 2H$ and $H \rightleftharpoons H^+ + e^-$. Boltzmann statistics are employed to calculate the partial molal Gibbs functions g_α and to develop analytic expressions for the ther-

modynamic properties ρ, h, D_P, D_T, C_P, and C_T. The variable cutoff employed by Patch[10] is used to truncate the divergent infinite series representing the electronic partition function of the hydrogen atom. Expressions for gas composition and thermodynamic properties are presented in Ref. 7.

Numerical Solution

For a specified cross-sectional area distribution, $A(x)$, Eqs. (7–9) reduce to the differential equations

$$\frac{d\bar{T}}{dx} = \frac{\bar{\rho}(1 - \bar{\rho}C_T)\bar{u}^3\, dA/dx - A(1 - D_T\bar{u}^2)S_E - (AD_T\bar{u}^3 - \dot{m}C_T)S_M}{\dot{m}C_P(1 - M^2)} \tag{11}$$

$$\frac{dP}{dx} = \frac{\bar{\rho}^2\bar{u}^2C_P\, dA/dx - \bar{u}AD_P S_E - A(\bar{\rho}C_P - D_P\bar{u}^2)S_M}{\bar{\rho}AC_P(1 - M^2)} \tag{12}$$

where

$$M = \frac{\bar{u}}{c_s} \quad \text{and} \quad c_s = \left(D_T + \frac{1 - \bar{\rho}C_T}{\bar{\rho}}\frac{D_P}{C_P}\right)^{-1/2}$$

while for a specified velocity distribution, $\bar{u}(x)$, Eqs. (7–9) reduce to the differential equations:

$$\frac{d\bar{T}}{dx} = \frac{1}{C_P}\left[C_T S_M - \frac{1}{\bar{\rho}\bar{u}}S_E - (1 - \bar{\rho}C_T)\bar{u}\frac{d\bar{u}}{dx}\right] \tag{13}$$

$$\frac{dP}{dx} = -S_M - \bar{\rho}\bar{u}\frac{d\bar{u}}{dx} \tag{14}$$

The numerical solution of either set of equations was obtained using fourth-order Runge-Kutta to march thru the duct, with x or $\bar{T}$ as the independent variable. For $A(x)$-specified ducts, the singularity at the sonic point restricts marching solutions, such as Runge-Kutta, to gas flows which are either subsonic or supersonic throughout the MHD generator. Inlet conditions for the generator gas flow included values for entrance pressure, magnetic field, and the temperature $\bar{T}_i$. Additionally, the entrance Mach number M_i was specified for $\bar{u}(x)$-specified ducts while D_i was specified for $A(x)$-specified ducts. Mass flow rate, duct width, loading parameter, wall temperature, and wall emissivity were specified constants. Equations (11–14), together with their respective inlet conditions and specified constants, are referred to as the gas dynamics computational (GDC) model.

At each step, electric work extracted and heat loss to the walls were calculated by

$$\Delta Q_w = (\Delta Q_w)_{\text{conv}} + (\Delta Q_w)_{\text{rad}} \tag{15}$$

$$\Delta w = \bar{H}_0(x) - \bar{H}_0(x + \Delta x) - (\Delta Q_w)_{\text{conv}} - \Delta Q_{\text{rad}} \tag{16}$$

where $\bar{H}_0 = \bar{h} + \bar{u}^2/2$. The parameters G, dB/B, and β_e were also calculated at each step through the generator. The heat loss to the walls per unit mass and electric work extacted per unit mass over the entire length of the MHD generator were given by the following summations over axial nodes k:

$$Q_{w,\text{tot}} = \sum_{k=2}^{m}\Delta Q_w = \sum_{k=2}^{m} Q_w(x_k) - Q_w(x_{k-1}) \tag{17}$$

$$w_{\text{tot}} = \sum_{k=2}^{m}\Delta w = \sum_{k=2}^{m} w(x_k) - w(x_{k-1}) \tag{18}$$

The magnetic field distribution $B(x)$ was calculated by approximating the shape of the superconducting coil as the intersection of two circles with a constant coil current density of 10^8 A/m^2 and using a generator wall plus cooling duct thickness of 5 cm.

Analysis of Radiative Heat Transfer

Governing Equations

For analysis of radiative transport within the hydrogen gas flow, the directional dependence of the radiative intensity is approximated by a truncated set of spherical harmonics, known as the P-1 approximation.[11] Integrating the spectral P-1 equations over a photon energy band j generates the three mean absorption coefficients a_{Pj}, a_{0j}, and a_{1j}, which are defined in Table 1. The mean absorption coefficient a_{Pj} is the familiar Planck mean for a particular band j and is a physical property of the gas. The mean absorption coeffcients a_{0j} and a_{1j} depend upon the solution of a particular problem and must be approximated in order to make the band-averaged P-1 equations useful.

Finkelman and Chien[12] show that $a_{0j} \sim a_{Pj}$ and $a_{1j} \sim a_{Rj}$ as the optical thickness approaches infinity, where a_{Rj} is the Rosseland mean over a particular band j. In the optically thin limit, the absorption means are roughly approximated by $a_{0j} \sim a_{Pj}$ and $a_{1j} \sim a_{Pj}$. In general it is expected that these absorption means will depend strongly on the temperature and reflective properties at gas boundaries. No studies (known to the authors) have been made concerning the behavior of the above mean absorption coefficients in the optically intermediate range, i.e., the optical thickness range between optically dense and optically thin. In this study, a_{0j} and a_{1j} are approximated by their optically thin or dense limits across a particular band j, depending on the optical thickness of the gas across that particular band.

Two- and three-dimensional analyses of the radiative transport are performed. The three-dimensional analysis is based on the actual MHD generator trapezoidal duct shape, shown earlier in Fig. 1. In the two-dimensional analysis, the actual MHD generator geometry is approximated by a diverging conical duct with a wall shape $r_w(x)$, as depicted in Fig. 2. The two-dimensional analysis further assumes an axisymmetric distribution of gas properties and axisymmetric wall boundary conditions, making the radiation problem two-dimensional. The temperature and density distributions are assumed to depend only on the axial coordinate x and are given by $\bar{T}(x)$ and $\bar{\rho}(x)$.

Table 1 Several mean absorption coefficients

If a_{sub} =	a_{Pj}	a_{0j}	a_{1j}	a_{Rj}	a_{mj}
Then f_{sub} =	$e_{b\omega}$	$I_{0\omega}$	$q_{\text{rad},\omega}$	$\frac{1}{a_\omega}\frac{\partial(e_{b\omega})}{\partial e_b}$	1

Where $a_{\text{sub}} = \dfrac{\int_{\Delta\omega j} a_\omega f_{\text{sub}}\, d\omega}{\int_{\Delta\omega j} f_{\text{sub}}\, d\omega}$

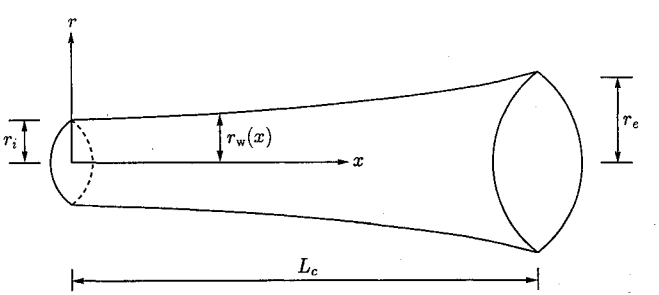

Fig. 2 Conical duct geometry.

For a given wall height $D_z(x)$ and width D_y, the wall shape for the conical duct is defined by

$$r_w(x) = \frac{1}{2}\left[\sqrt{\frac{D_y D_z(x)}{\pi}} + \frac{D_y D_z(x)}{D_y + D_z(x)}\right] \tag{19}$$

where the first term within the brackets represents the local cone radius for equal cross-sectional areas (between the trapezoidal duct and conical duct), and the second term represents the local cone radius for equal mean beam lengths. Also, the condition $L_c = L$ is used so that axial gradients in $\bar{T}$ and $\bar{\rho}$ are equivalent in the trapezoidal and conical ducts.

The band-averaged P-1 elliptic partial differential equation for I_{0j} is given by

$$\frac{1}{r}\frac{\partial}{\partial r}\left(\frac{r}{a_j^*}\frac{\partial I_{0j}}{\partial r}\right) + \frac{\partial}{\partial x}\left(\frac{1}{a_j^*}\frac{\partial I_{0j}}{\partial x}\right) = 3a_{Pj}(I_{0j} - 4e_{bj}) \tag{20}$$

in axisymmetric cylindrical coordinates, and by

$$\frac{\partial}{\partial x}\left(\frac{1}{a_j^*}\frac{\partial I_{0j}}{\partial x}\right) + \frac{\partial}{\partial y}\left(\frac{1}{a_j^*}\frac{\partial I_{0j}}{\partial y}\right) + \frac{\partial}{\partial z}\left(\frac{1}{a_j^*}\frac{\partial I_{0j}}{\partial z}\right) = 3a_{Pj}(I_{0j} - 4e_{bj}) \tag{21}$$

in three-dimensional Cartesian coordinates, where the mean absorption coefficient a_j^* is defined by

$$a_j^* = \begin{cases} a_{Pj} & \text{Gas is optically thin over band } j \\ a_{Rj} & \text{Gas is optically dense over band } j \end{cases}$$

For a diffuse, semigray surface, in which the value of the spectral wall emissivity $\varepsilon_{s\omega}$ is constant over each band j, the band-averaged P-1 boundary condition for I_{0j} is given by

$$-(\boldsymbol{q}_{\text{rad},j}\cdot\hat{\boldsymbol{n}}_s)|_s = \left(\frac{\nabla I_{0j}}{3a_j^*}\cdot\hat{\boldsymbol{n}}_s\right)\bigg|_s = \frac{1}{2}\frac{\varepsilon_{s,j}}{2 - \varepsilon_{s,j}}[I_{0j}|_s - 4e_{bj}(T_s)] \tag{22}$$

Numerical Solution

For each band j, Eq. (20) (two-dimensional analyis) or Eq. (21) (three-dimensional analysis) was solved numerically for I_{0j}, assuming the temperature and density distributions were known throughout the gas. For the two-dimensional analysis, the code developed for the solution of Eq. (20) was a modification of a previous code.[13] Note that the temperature-density dependent mean absorption coefficients a_{Pj} and a_j^* may vary throughout the gas. The inlet and exit planes of the duct were approximated as blackbodies at uniform temperatures T_{ip} and T_{ep}, respectively. The inlet plane blackbody temperature T_{ip} was set equal to $\bar{T}_i$. This is a reasonable value since, at the generator inlet, the temperature gradient is typically decreasing and temperatures are so high that the gas is essentially a blackbody radiator. The exit plane blackbody temperature T_{ep} was set equal to 294 or 4 K, depending on vehicle orientation with respect to the Earth. Since gas temperatures at the generator exit (8000–12,000 K) are so much larger than either of these T_{ep} values, there is essentially no difference (typically less than 0.1%) in the radiative transport between $T_{ep} = 294$ K and $T_{ep} = 4$ K. The walls of the conical duct were treated as gray-diffuse surfaces with a uniform T_w. The blackbody emissive power $e_{bj}(T)$ for each band j was calculated using the polynomial curve fits recommended by Wiebelt.[14]

For the two-dimensional analysis, the computational grid for numerical simulation consisted of many nonoverlapping control volumes. The majority of the control volumes were circular rings of rectangular cross section. Along the curved diverging surface of the cone, rings of triangular cross section were used to approximately fit the shape of the gas boundary. Control volumes were uniformly spaced along the x axis, but were uniform along the r axis only in the region $0 \le r \le r_i$. For the three-dimensional analysis, symmetry about the y and z axes was assumed; thus, only one-fourth of the duct volume, defined by $0 \le x \le L$, $0 \le y \le \frac{1}{2}D_y$, and $0 \le z \le \frac{1}{2}D_z$, was analyzed. The same type of r-x grid described above was used at each y location, except that z replaces r, and the wall shape is given by $\frac{1}{2}D_z(x)$. Control volumes were thus rectangular boxes for a majority of the computational grid, with trapezoidal volumes used to approximately fit the diverging wall shape along $z = \frac{1}{2}D_z$; the flat wall $y = \frac{1}{2}D_y$ was fitted exactly.

A set of discretized algebraic equations for I_{0j} was derived by integrating Eq. (20) or Eq. (21) over each control volume. Equation (22) was employed for control volume surfaces along the boundary of the gas. The local radiative heat flux $q_{w,\text{rad}}$ into the duct wall from a bounding control volume was computed using Eq. (22), summed over all j bands. Also, applying the band-averaged P-1 relation

$$\nabla\cdot\boldsymbol{q}_{\text{rad},j} = 4a_{Pj}e_{bj} - a_{Pj}I_{0j} \tag{23}$$

at x locations corresponding to grid points and summing over all j bands, the quantities $\bar{s}_{\text{rad}}$ and ΔQ_{rad} were calculated for use in the gas dynamics computational model. The integrals for $\bar{s}_{\text{rad}}$ and ΔQ_{rad} reduce to summations along the r axis for the two-dimensional analysis, or along the y and z axes for the three-dimensional analysis, since the discretization assumes $\nabla\cdot\boldsymbol{q}_{\text{rad}}$ is constant over each control volume. Richardson extrapolation to zero grid spacing for several test cases indicated that the gray isothermal P-1 solution for typical conical ducts was within 5% of the zero grid spacing solution for approximately 500 control volumes. The numerical solution procedures discussed above are referred to as the two- and three-dimensional radiation heat transfer computational (RHTC) models.

Data for the spectral variation of the absorption coefficient of hydrogen gas at 672 temperature-density states was generated[15] for a temperature grid of 0.25–1.8 eV in steps of 0.05 eV, a density grid of 10^{-8}–10^{-4} g/cm^3 in steps of 1, 2, 4, 6, 8 per decade (i.e., 1×10^{-8}, 2×10^{-8}, . . . , 8×10^{-5}, 1×10^{-4}), and a photon energy grid of 0.0035–50 eV in steps of 0.0035 eV for $\omega \le 14$ eV (region with significant line radiation), followed by steps of 0.1 eV out to 50 eV (continuum radiation only). Radiation intensities of the hydrogen gas and generator walls are insignificant in the regions $\omega > 50$ eV and $\omega < 0.0035$ eV for the temperature and density ranges considered here. Solution of the band-averaged P-1 equations requires that the spectral behavior of the absorption coefficient be approximated by a finite number of bands. An 8-band model was selected as the minimum number of bands required to adequately model the spectral variation of a_ω. The photon energy values defining the band intervals are given in Table 2. Values for the absorption means a_{Pj}, a_{Rj}, and a_{mj} (the arithmetic mean) were computed using the trapezoid rule to numerically integrate across each band j.

Table 2 Photon energy intervals for 8-band model of spectral absorption coefficient

ω Band	ω Interval, eV
1	0.0035–1.6345
2	1.6345–2.2680
3	2.2680–2.6950
4	2.6950–7.0000
5	7.0000–10.9620
6	10.9620–12.3760
7	12.3760–12.8870
8	12.8870–50.0000

This study treats each band j as optically dense or optically thin. For an optically dense isothermal gas, l_{mb} represents a characteristic length for radiative transport and is used here to define the optical thickness of the gas over a band j, $\mathbb{O}_j = a_{mj} l_{mb}$. An optical thickness of five was deemed a reasonable value for the borderline thickness between optically dense and optically thin. Thus, those bands with $\mathbb{O}_j < 5$ were treated as optically thin, and those bands with $\mathbb{O}_j > 5$ were treated as optically dense. Using this criterion, with a_{mj} evaluated at an estimated average state of the gas over the length of the MHD generator and an estimated $l_{mb} = 7.7$ cm, all bands except 3 and 4 were treated as optically dense. Band 1 and bands 5–7 are very dense, while bands 2 and 3 are essentially on the borderline between dense and thin.

Coupled Gas Dynamics/Radiative Heat Transfer Solution

Coupling the gas dynamics and radiative heat transfer computational models produces a system of nonlinear algebraic equations for the dependent variables $\tilde{T}_k$, $\tilde{\rho}_k$, and $(I_{0j})_l$, where k corresponds to axial nodes, j corresponds to photon energy bands, and l corresponds to nodes in the computational grid for the conical duct. Coupled solutions using the three-dimensional P-1 code were not attempted due to CPU limitations; the three-dimensional analysis of radiative transport was used only to test the accuracy of the two-dimensional P-1 code for a given solution. For a typical case of 30 axial nodes, 500 nodes in the conical duct computational grid, and 8 photon energy bands, there are 4060 nonlinear equations and unknowns. The iterative procedure used to couple gas dynamics and radiative transport for a specified cross-sectional area distribution $A(x)$ is as follows:

1) Calculate $\tilde{T}(x)$ and $\tilde{\rho}(x)$ from the gas dynamics computational (GDC) model using an initial guess for $\tilde{s}_{rad}(x)$.

2) Calculate a new $\tilde{s}_{rad}(x)$ from the radiative heat transfer computational (RHTC) model using the $\tilde{T}(x)$ and $\tilde{\rho}(x)$ generated by the GDC model.

3) Calculate new $\tilde{T}(x)$ and $\tilde{\rho}(x)$ from the GDC model using the $\tilde{s}_{rad}(x)$ generated by the RHTC model.

4) Repeat steps 2 and 3 until the changes in $\tilde{T}(x)$, $\tilde{\rho}(x)$, and $\tilde{s}_{rad}(x)$ satisfy the convergence criterion.

In step 3, values for $\tilde{T}$, $\tilde{\rho}$, $\tilde{s}_{rad}$, S_E, and S_M at each axial node k were determined by a local relaxation method of the form

$$Y_k = Z_k + R(\tilde{Y}_k - Z_k) \tag{24}$$

in which $\tilde{Y}_k$ is the new value calculated, Z_k is the relaxed value from the previous iteration, R is the underrelaxation factor (never greater than one), and Y_k is the relaxed value actually used for the required quantity during the current iteration. The following algorithm was used to assign local relaxation factors:

$$R = \begin{cases} R_{high}; & |\delta| > 0.5 \\ R_{low}; & |\delta| < 0.5 \end{cases} \tag{25}$$

where the percent change δ was defined by

$$\delta = \begin{cases} \dfrac{\tilde{Y}_k - Z_k}{\tilde{Y}_k}; & |\tilde{Y}_k| > |Z_k| \\ \dfrac{\tilde{Y}_k - Z_k}{Z_k}; & |\tilde{Y}_k| < |Z_k| \end{cases} \tag{26}$$

and the constants R_{high} and R_{low} represent high and low values for the under-relaxation factor of a particular variable. The constants R_{high} and R_{low} are typically of the order 10^{-1} and 10^{-2}, respectively. The convergence criterion imposed on $\tilde{T}(x)$, $\tilde{\rho}(x)$, and $\tilde{s}_{rad}(x)$ required that the error from one iteration to the next, in each distribution, fall below a specified tolerance (typically 10^{-3}). The error for each distribution was represented by the maximum nodal error (m.n.e.) of that distribution

$$\text{m.n.e.}[Y(x)] = \max\left(\left|\frac{\tilde{Y}_k - Z_k}{\tilde{Y}_k}\right|\right)_{k=1 \text{ to } m} \tag{27}$$

where $\tilde{Y}_k$ was the true (i.e., not relaxed) value at node k for the current iteration, and Z_k was the value at node k from the previous iteration.

Optimal Design

Only one application of the MHD generator open-cycle power supply is considered here. Designs are developed which could serve as onboard electric power supplies for the Apollo Lightcraft,[16,17] a small transatmospheric vehicle for transport to low Earth orbit. The advanced combined-cycle engine of this lightcraft requires large amounts of electric power (~1250 MW_e) during the hypersonic portion of its launch trajectory, in which shock-heated air flowing over the vehicle forebody is accelerated through an annular MHD accelerator duct under the application of electric and magnetic fields.

The optimal design of an MHD generator power supply for the Apollo Lightcraft may be stated mathematically as follows:

Maximize the objective function $F(X) = w_{tot}/Q_N$ subject to the inequality constraints $g_K(X) \geq 0$

$$g_1 = 1 - \frac{Q_{w,tot}}{200 \text{ MJ/kg}}$$

$$g_2 = 1 - \frac{\max(q_w)}{450 \text{ MW/m}^2}$$

$$g_3 = 1 - \frac{80 \text{ MW}}{\dot{m} w_{tot}}$$

$$g_4 = 1 - \frac{0.0108 \text{ bar}}{P_e}$$

$$g_5 = 1 - \frac{1000 \text{ K}}{\tilde{T}_e}$$

$$g_6 = 1 - \frac{L}{1.5 \text{ m}}$$

$$g_7 = 1 - 4\frac{\max(D_e, D_y)}{L}$$

$$g_8 = 1 - \frac{0.01 \text{ m}}{\min(D_i, D_y)}$$

$$g_9 = 1 - \frac{\max(\beta_e)}{2}$$

$$g_{10} = 1 - \frac{\max\left(\dfrac{dB}{B}\right)}{0.1}$$

$$g_{11} = 1 - \frac{\max(M)}{0.92}$$

for the design variables X

$$X = (\bar{T}_i, P_i, B_i, \dot{m}, D_y, T_w, K, M_i \text{ or } D_i, \bar{T}_e \text{ or } L)$$

$$10^3 \le \bar{T}_i \le 20{,}000 \text{ K}$$

$$20 \le P_i \le 200 \text{ bar}$$

$$10^{-6} \le B_i \le 15 \text{ T}$$

$$10^{-6} \le \dot{m} \le 5 \text{ kg/s}$$

$$0.01 \le D_y \le 0.255 \text{ m}$$

$$500 \le T_w \le 2500 \text{ K}$$

$$10^{-6} \le K \le 0.98$$

$$10^{-6} \le M_i \le 0.92$$

$$0.01 \le D_i \le 0.225 \text{ m}$$

$$1000 \le \bar{T}_e \le 20{,}000 \text{ K}$$

$$10^{-6} \le L \le 1.0 \text{ m}$$

Note that the variables in $F(X)$ and $g_K(X)$, such as w_{tot} and $Q_{w,\text{tot}}$, are determined by the GDC model and are therefore, implicitly, functions of X. The above inequality constraints are due to both assumptions made in the mathematical model describing the MHD generator gas flow and design requirements for the Apollo Lightcraft. Formulation of constraints and bounds on the design variables are discussed in detail in Ref. 7. The above problem statement applies to $\bar{u}(x)$- or $A(x)$-specified designs, and to GDC models which integrate in $\bar{T}$ or x.

In order to limit radiative wall heat fluxes to a tolerable level (less than 100 MW/m^2), wall emissivities near 10^{-2} are required. Emissivities of 10^{-3} to 10^{-4} may be possible[18] in the low uv spectrum for insulator sections of the MHD generator walls through the application of thin multilayer dielectric coatings (e.g., 0.5 mm of MgO/MgF_2) over the insulator surface. Similar treatment of electrode surfaces may not be possible due to the suspected drop in electrical surface conductivity for dielectric-coated electrodes. For typical generator designs, maximum radiative intensities generally occur in the visible and low ultraviolet frequencies. Based on these considerations, the design value of $\varepsilon_w = 10^{-3}$ was chosen. The effect of larger wall emissivities, which might be caused by gas/surface interactions and/or larger electrode wall emissivities, is considered in the next section (Fig. 5).

The following solution strategy was used to find optimal MHD generator designs:

1) Using the GDC model only, with estimates of $\bar{s}_{\text{rad}}$, ΔQ_{rad}, and $q_{w,\text{rad}}$, and $\bar{u}(x)$ = a specified constant, generate a feasible starting point by trial and error optimization.

2) Using the generalized reduced gradient code OPT 3.2,[19] find a local optimum starting from the above feasible generator design, again using only the GDC model, with some estimates of $\bar{s}_{\text{rad}}$, ΔQ_{rad} and $q_{w,\text{rad}}$, and $\bar{u}(x)$ = a specified constant. OPT 3.2 is capable of minimizing a single nonlinear objective function subject to several nonlinear equality and/or inequality constraints as a function of several design variables.

3) For the design variables and discretized area distribution $A(x_k)$ corresponding to the above local optimum, find the coupled gas dynamics/radiative heat transfer solution using the iterative method to couple the GDC model and RHTC model.

Since thermophysical properties depend strongly on temperature, the GDC model used $\bar{T}$ as the marching variable in steps 1 and 2, while in step 3, x was the marching variable. Only the two-dimensional RHTC model was used to find coupled solutions; however, differences in the radiative loss distribution $\bar{s}_{\text{rad}}(x)$ between the two- and three-dimensional RHTC models for typical MHD generator conditions were on the order of 10–20% for most of the duct length, so the two-dimensional RHTC model served as a reasonable design tool. Values for $D_z(x)$ and $r_w(x)$ at x values between the axial nodes x_k, which are required in step 3, were calculated using cubic spline interpolations.

Results

A systematic search for feasible starting points began by analyzing generator designs which enforced a constant velocity $\bar{u}$ and used the temperature $\bar{T}$ as the marching variable in the GDC model. Also, since the coupled gas dynamics/radiative heat transfer solution was difficult in general, the initial search for feasible designs used the following approximations for the required radiative terms:

$$q_{w,\text{rad}}(x) = 3.0 \text{ MW/m}^2 \quad \text{for all } x$$

$$\bar{s}_{\text{rad}}(x) = 1.0 \text{ GW/m}^3 \quad \text{for all } x$$

$$\Delta Q_{\text{rad}}(x) = \bar{s}_{\text{rad}}(x)[V(\Delta x)/\dot{m}]$$

The above values were expected to underestimate actual values and were chosen based on preliminary coupled solutions of $A(x)$-specified generators.

Using the feasible design with the highest extraction ratio as a starting point for the optimization code OPT 3.2, an optimal generator design (referred to as DS 1) was found for the approximate distribution $\bar{s}_{\text{rad}}(x) = 1.0$ GW/m^3. Exit values of this design (which are expected to be most sensitive to grid spacing since this is a marching solution), calculated by the GDC model with x as the marching variable for $m = 30$ axial nodes, were compared with exit values extrapolated to zero grid spacing using solutions for $m = 40$, 70, and 100; values for $\bar{T}_e$, P_e, $Q_{w,\text{tot}}$, w_{tot}, and other exit quantities for $m = 30$ were within 2% of the values extrapolated to zero grid spacing.

The coupled gas dynamics/radiative heat transfer solution using the generator design variables and area distribution corresponding to design DS 1 was accomplished using the iterative method described above to couple the GDC and two-dimensional RHTC models. A total of 1547 iterations was

Table 3 Near-optimal MHD generator design

Design variables	
$\bar{T}_i$ = 17,961 K	T_w = 2,500 K
P_i = 50.06 bars	K = 0.98
B_i = 5.021 T	L = 0.8550 m
$\dot{m}$ = 0.3950 kg/s	M_i = 0.2619
D_y = 0.2137 m	ε_w = 0.001
Resulting design	
H_R = 35.54%	max{dB/B} = 0.0063
w_{tot} = 323.98 MJ$_e$/kg	max{β_e} = 0.4395
$Q_{w,\text{tot}}$ = 156.8 MJ/kg	max{θ} = 10.79°
$q_{w,i}$ = 452.9 MW/m^2	L/D_y = 4.001
Q_{tot} = 248.9 MJ/kg	L/D_e = 4.924
$\dot{W}_{\text{gen}}$ = 128.0 MW$_e$	$\bar{T}_e$ = 10,462 K
V_{gen} = 1.217 × 10^4 cm^3	P_e = 7.844 bars
Q_N = 911.5 MJ/kg	Re_{avg} = 1.54 × 10^5
$(\bar{J}_y)_i$ = 249.6 amps/cm^2	D_i = 1.694 cm
$(\bar{E}_y)_i$ = 19.09 kV/m	D_e = 0.1736 m
L_{cnt} = 0.3044 m	$\bar{u}_i$ = 3,883 m/s
m = 30 axial nodes	$\bar{u}_e$ = 1,184 m/s
l_{mb} = 9.323 cm	max{$\Delta\bar{T}$} = 367.7 K

required for the m.n.e. of the distributions $\bar{T}(x)$, $\bar{\rho}(x)$, and $\bar{s}_{rad}(x)$ to fall below a tolerance of 10^{-3}. All computations were performed on a DEC VAX 6320. The resulting performance for the coupled solution of this generator design is summarized in Table 3. This design is termed a near-optimal design since further optimization studies using OPT 3.2 and the GDC model with an approximate $\bar{s}_{rad}(x)$ distribution might be accomplished using the $\bar{s}_{rad}(x)$ distribution found from the above coupled solution as the approximate distribution. Several cycles of this procedure might be necessary to find a true optimum within a certain range of design variables.

Figure 3 shows the axial variation of several generator quantities of interest. All quantities shown vary smoothly and, except for M, exhibit monotonic axial behavior. The radiative wall heat flux $q_{w,rad}$ accounts for only 1.3–2.5% of the total wall heat flux q_w throughout the generator; thus, the axial wall heat flux distribution $q_w(x)$ shown in Fig. 3a represents essentially $q_{w,conv}(x)$. The heat flux into the generator walls ranges from 452.9 MW/m^2 at the generator entrance down to 18.51 MW/m^2 at the exit.

As shown in Fig. 3c, increases in $Q_{w,conv}$, $Q_{w,rad}$, and w are fairly constant throughout most of the duct, but level off near the exit. This leveling off in electric work extracted indicates that the design makes efficient use of the generator volume in terms of energy extraction, since further increases in generator length will not significantly increase w_{tot}. Although $\bar{J}_y$ and $\bar{E}_y$ decrease through the generator, the specific electric work Δw extracted over an axial length Δx remains fairly constant since Δw is proportional to $V(\Delta x)$, which increases due to the increasing cross-sectional area $A(x)$. Similarly, although convective and radiative wall heat fluxes decrease through the generator, surface areas over an axial length Δx increase due to the increasing $A(x)$, thus maintaining fairly constant convective and radiative heat losses to the walls, $\Delta Q_{w,conv}$ and $\Delta Q_{w,rad}$.

The three-dimensional radiative transport analysis for the above generator design was calculated using the same distributions $\bar{T}(x)$, $\bar{\rho}(x)$, and $A(x)$ as the near-optimal design, and was compared with the two-dimensional solution for the corresponding conical duct. The three-dimensional RHTC model employed 30 axial nodes and 1980 control volumes compared to 30 axial nodes and 495 control volumes for the two-dimensional RHTC model. A maximum percent difference of 7% between the radiative wall heat flux computed by the two-dimensional analysis and the perimeter-averaged radiative wall

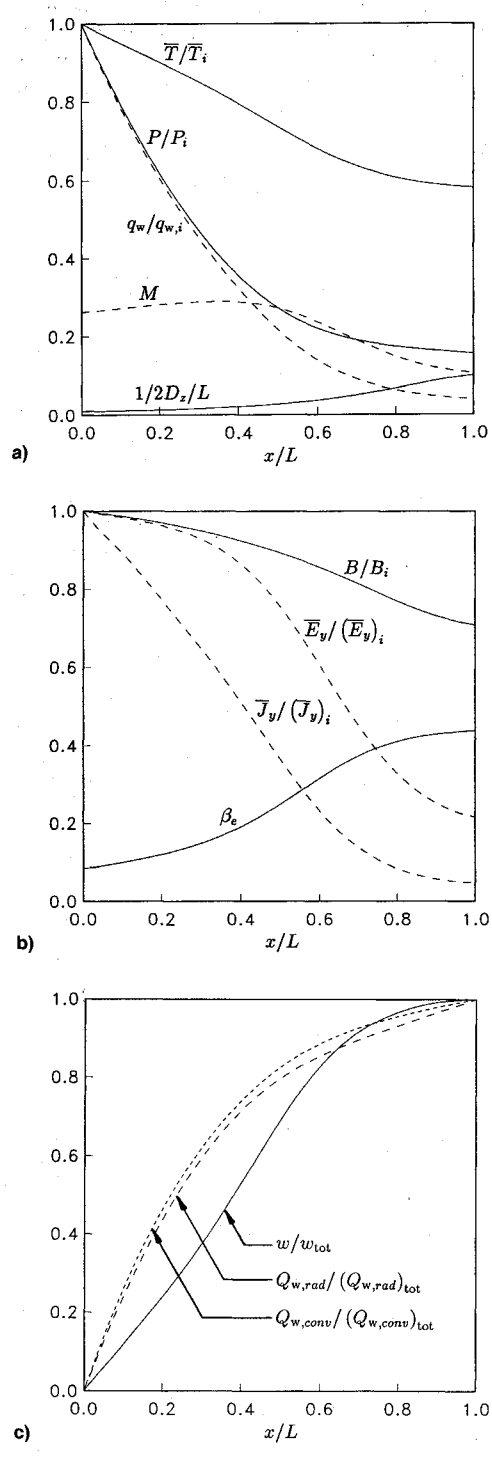

Fig. 3 Axial distributions for near-optimal generator design.

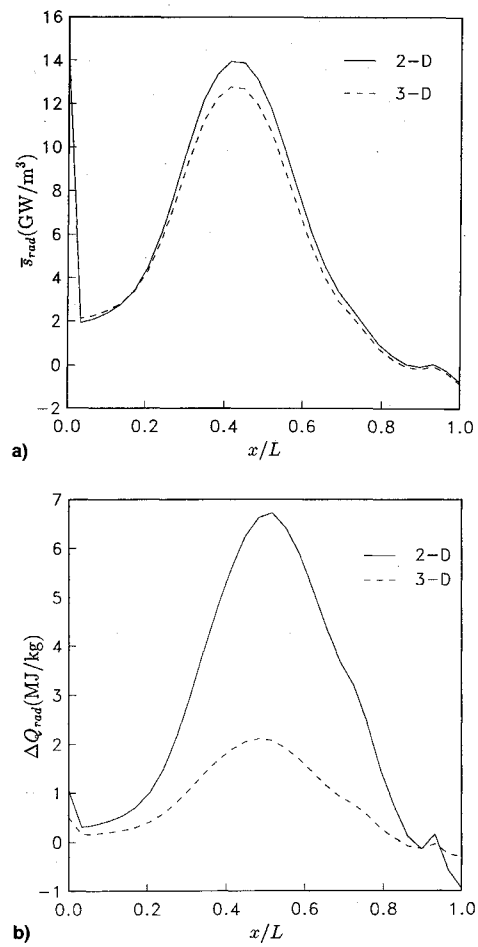

Fig. 4 Axial distributions of: a) $\bar{s}_{rad}$ and b) ΔQ_{rad} for near-optimal generator design calculated by the two- and three-dimensional RHTC models.

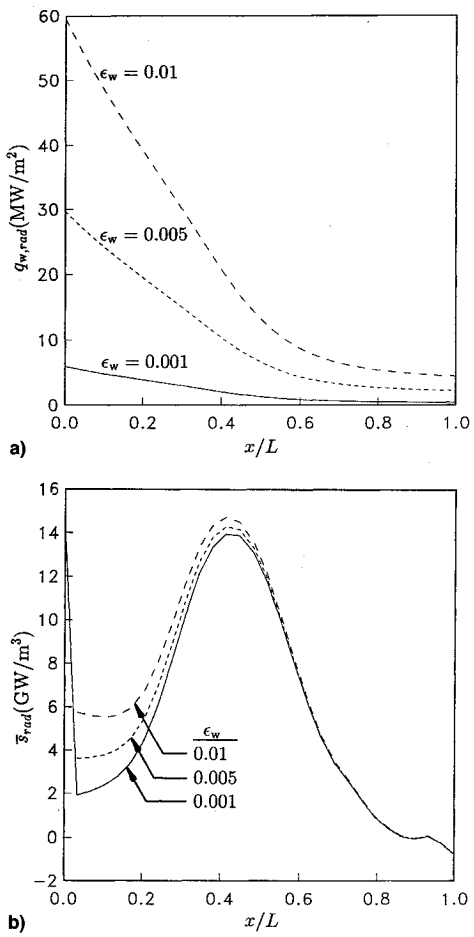

Fig. 5 Axial distributions of: a) $q_{w,rad}$ and b) $\bar{s}_{rad}$ for wall emissivities of ε_w = 0.01, 0.005, and 0.001.

heat flux computed by the three-dimensional analysis occurred at the generator exit. The two-dimensional solution for the radiative loss term $\bar{s}_{rad}(x)$ compares fairly well with the three-dimensional solution, as shown in Fig. 4a. The shape of the distribution $\bar{s}_{rad}(x)$ is due mainly to the contributions from the ω bands $j = 4$ and $j = 5$.

Figure 4b shows the large overestimate by the two-dimensional analysis of the volume radiative loss term ΔQ_{rad} due to larger volumes $V(\Delta x)$, relative to the three-dimensional analysis, over most of the generator length. Values for $q_{w,rad}$ and ΔQ_{rad} are not required for the solution of Eqs. (7–10); these terms are calculated only in order to determine wall heat loads and electric work extracted. Thus, values for w and w_{tot}, as shown in Table 3 and Fig. 3c, are based on the three-dimensional analysis values of ΔQ_{rad}.

The effect of higher wall emissivities is shown in Fig. 5. For $\bar{s}_{rad}$, the maximum percent difference between the case $\varepsilon_w = 0.001$ (the design point) and $\varepsilon_w = 0.01$ occurs at the duct entrance; for 66% of the axial length the percent difference in $\bar{s}_{rad}$ is below 10%. This indicates that generator designs similar to the optimal design analyzed here should be possible even if wall emissivities cannot be reduced below 0.01. However, radiative wall heat fluxes will increase by a factor of about 10 and the maximum wall heat flux $q_{w,i}$ will increase by about 12%.

Conclusions

The results of this study indicate that equilibrium, ultrahigh temperature MHD generators can be designed as efficient, compact, open-cycle power supplies, but are subject to very harsh thermal environments. Maximum wall heat fluxes and total wall heat loads are on the order of 450 MW/m² and 62 MW, respectively. The convective wall heat flux accounts for over 95% of the total wall heat flux throughout the generator. Extraction ratios of 35.5% and power densities of 10,500 MW_e/m^3 are theoretically possible at power levels of 128 MW_e and specific energy levels of 324 MJ_e/kg of hydrogen. The major advantages of this class of generators relative to conventional, lower-temperature MHD generators are exceptionally high-power densities and high specific energy outputs; this results in compact (on the order of 20 × 20 × 100 cm) electric power supplies delivering reasonably large power outputs and requiring relatively small amounts of fuel. Lower-temperature, combustion-driven MHD generators are characterized by maximum power densities and specific energy outputs of 10–500 MW_e/m^3 and 1–4 MJ_e/kg, respectively.

High working fluid temperatures (10,000–20,000 K) eliminate the need for seeding, but cause radiative transport to become an important phenomenon of the gas flow and push convective heat fluxes into generator walls to levels of 18.5 MW/m² at the generator exit up to 450 MW/m² at the entrance, for turbulent flow throughout the generator. Maintaining wall temperatures of 2500 K will require cryogenic coolants and convective heat transfer coefficients of 18,000 W/m² K to 184,000 W/m² K—pushing the limits of current heat transfer technology. The major radiative losses occur along the generator exit plane and are characterized by average radiative heat fluxes of 985 MW/m² and total heat losses of 93 MJ/kg of hydrogen, for low-temperature (300 K) surroundings. Attaching insulating walls segments at the generator exit to reduce eddy-current end losses may also reduce radiative losses by increasing the effective blackbody temperature of the generator exit plane.

On the order of 70% or more of the total radiative wall heat flux is produced within the high visible and low UV photon energy range of 2.7–10.962 eV; this corresponds essentially to the Lyman series line ω_{12} = 10.204 eV and its wings, and the fairly transparent photon energy band preceding it. Wall emissivities of 10^{-2} are sufficient to keep wall radiative heat fluxes below 60 MW/m²; however, it may be possible to reduce radiative wall heat fluxes by almost an order of magnitude if wall emissivities of 10^{-3} are possible.

Acknowledgments

This work was partially supported by NASA Lewis Research Center under Contract NAG 3-916, entitled Futuristic Propulsion Systems, with R. W. Luidens as program manager. The authors wish to thank Richard J. Rosa of Montana State University for his assistance in the development of the gas dynamics model and Norman H. Magee of Los Alamos National Laboratory for producing the hydrogen absorption coefficient data.

References

[1]Jeng, S.-M., and Keefer, D., "Theoretical Evaluation of Laser-Sustained Plasma Thruster Performance," *Journal of Propulsion and Power*, Vol. 5, No. 5, 1989, pp. 577–581.

[2]Jeng, S.-M., and Keefer, D. R., "Numerical Study of Laser-Sustained Hydrogen Plasmas in a Forced Convective Flow," *Journal of Propulsion and Power*, Vol. 3, No. 3, 1987, pp. 255–262.

[3]Myrabo, L. N., "Advanced Beamed-Energy and Field Propulsion Concepts," The BDM Corp., BDM/W-83-225-TR, McLean, VA, 1983.

[4]Rosa, R. J., and Myrabo, L. N., "Ultra-Performance Closed-Cycle Gas Core Reactors for Orbit Raising," Vol. 89, Progress in Astronautics and Aeronautics, AIAA, New York, 1984, pp. 460–476.

[5]Myrabo, L. N., Kaminski, D. A., Rosa, R. J., and Moder, J. P., "Concept Analysis of a Novel Integrated Directed Energy Power System," Wright Aeronautical Lab., AeroPropulsion Lab., Technical Report, Subcontract 19X-2745909, Sept. 1987.

[6]Mitchner, M., and Kruger, C. H., Jr., *Partially Ionized Gases*, Wiley, New York, 1973, pp. 391–397, 406–409.

[7]Moder, J. P., "Analysis and Design of an Ultra-High Temperature, Hydrogen-Fueled MHD Generator as an Open Cycle Power Supply," Ph.D. Dissertation, Rensselaer Polytechnic Inst., New York,

Aug. 1990.

[8]Rosa, R. J., personal communication, Montana State Univ., Bosemann, MT, 1986.

[9]Yos, J. M., "Transport Properties of Nitrogen, Hydrogen, Oxygen, and Air to 30,000 K," AVCO Corp., RAD-TM-63-7, Wilmington, MA, March 1963.

[10]Patch, R. W., "Components of a Hydrogen Plasma Including Minor Species," NASA TN D-4993, Jan. 1969.

[11]Cheng, P., "Dynamics of a Radiating Gas with Application to Flow over a Wavy Wall," *AIAA Journal*, Vol. 4, No. 2, 1966, pp. 238–245.

[12]Finkleman, D., and Chien, K. Y., "Semigrey Radiative Transfer," *AIAA Journal*, Vol. 6, No. 4, 1968, pp. 755–758.

[13]Kaminski, D. A., "Radiative Transfer from a Gray, Absorbing-Emitting, Isothermal Medium in a Conical Enclosure," *Journal of Solar Energy Engineering*, Vol. 111, Nov. 1989, pp. 324–329.

[14]Wiebelt, J. A., *Engineering Radiation Heat Transfer*, Holt, Rinehart and Winston, New York, 1966.

[15]Magee, N. H., personal communication, Los Alamos National Lab., NM, 1988.

[16]Moder, J. P., Blandino, J., Frazier, S. R., and Myrabo, L. N., "Laser-Energized MHD Generator for Hypersonic Electric Air-Turborockets," AIAA Paper 87-1816, June 1987.

[17]Minucci, M. A. S., and Myrabo, L. N., "Phase Distortion in a Propulsive Laser Beam due to Aero-Optical Phenomena," *Journal of Propulsion and Power*, Vol. 6, No. 4, 1990, pp. 416–425.

[18]Sparks, M., "Assessment of Materials and Coatings Requirements for UV Laser Optics," The BDM Corp., Defense Advanced Research Projects Agency, BDM/W-81-447-TR, Aug. 1981.

[19]Gabriele, G. A., and Beltracchi, T. J., "OPT 3.2: A Nonlinear Programming Code Based on the Generalized Reduced Gradient Method," Dept. of Mechanical Engineering, Aeronautical Engineering and Mechanics, Rensselaer Polytechnic Inst., New York, 1988.